crystals

MDPI

Article

Printable Silicone-Based Emulsions as Promising Candidates for Electrically Conductive Glass-Ceramic Composites

Annalaura Zilio and Enrico Bernardo *

Department of Industrial Engineering, University of Padova, 35131 Padova, Italy; annalaura.zilio@phd.unipd.it
* Correspondence: enrico.bernardo@unipd.it

Abstract

The Na_2O-SrO-SiO_2 system shows promise in the development of glasses that can be transformed into electrically conductive glass ceramics. The conventional processing of such materials usually involves the synthesis of a parent glass, followed by a complex devitrification treatment. This study proposes a simplified approach based on the use of preceramic polymers, namely silicone resins combined with oxide fillers. These systems yield silicate-based ceramics through direct heat treatment, replicating the phase assembly of traditional glass ceramics with no need for prior glass melting. A printable formulation was developed by mixing a silicone resin with an acrylate-based photocurable resin, sodium nitrate and strontium carbonate. The resulting 'suspension-emulsion' was later shaped into monolithic components using digital light processing. After pyrolysis in nitrogen atmosphere, the components transformed into $SrSiO_3$ crystals embedded in a composite matrix, in turn composed of glass and turbostratic carbon (the latter specifically offered by the silicone polymer). This combination of crystalline silicates and carbon resulted in measurable electrical conductivity. This study confirms that silicone-derived systems can serve as effective precursors for conductive glass-ceramic analogues, providing an alternative to conventional methods with single-step processing. This approach enables structural shaping through 3D printing and the development of functional properties suitable for electronic or electrochemical applications.

Keywords: conductive glass-ceramic; polymer derived ceramics; ceramic additive manufacturing; Na_2O-SrO-SiO_2 system

check for updates

Academic Editor: Jiamin Wu

Received: 30 June 2025
Revised: 12 October 2025
Accepted: 13 October 2025
Published: 14 October 2025

Citation: Zilio, A.; Bernardo, E. Printable Silicone-Based Emulsions as Promising Candidates for Electrically Conductive Glass-Ceramic Composites. *Crystals* **2025**, *15*, 885. https://doi.org/10.3390/cryst15100885

Copyright: © 2025 by the authors. Licensee MDPI, Basel, Switzerland. This article is an open access article distributed under the terms and conditions of the Creative Commons Attribution (CC BY) license (https://creativecommons.org/licenses/by/4.0/).

1. Introduction

Glass-ceramics are a class of glass-ceramic composites in which one or more crystalline phases are dispersed within a residual glassy matrix. This unique microstructure enables a combination of properties not typically achievable in either glasses or fully crystalline ceramics, such as tailored thermal expansion, mechanical strength, and ionic or electronic conductivity [1]. In particular, glass-ceramics based on the Na_2O-SrO-SiO_2 system have shown potential for high-temperature ionic conduction [2–5], making them promising candidates for applications in sensors, solid-state batteries, and electrochemical devices [6–8].

Recent studies, such as the work by Smeacetto et al. [2], have demonstrated that fast-quenched samples in this compositional system outperform traditional solid-state synthesis and $SrSiO_3$-$Na_2Si_2O_5$ composites in terms of ionic conductivity and structural stability. These fast-quenched materials exhibit enhanced crystallization behaviour, with crystalline domains acting as nucleation sites for the recrystallization of $Na_2Si_2O_5$, a phase

that contributes significantly to Na^+ ion transport. A notable conductivity of 10^{-1} S·cm^{-1} at 750 °C has been reported, along with the reversible formation of the $Na_2Si_2O_5$ phase, offering the possibility of regenerating ionic pathways upon thermal cycling [2,9].

Despite these favourable properties, conventional glass-ceramic processing is often complex and resource-intensive [10]. It typically requires the initial formation of a parent glass via melt-quenching, followed by a controlled heat treatment to induce crystallization. This multi-step process limits scalability, increases production costs, and restricts design flexibility, particularly for complex geometries [2,11].

To address these challenges, the so-called polymer-derived ceramics (PDCs) approach [12] may offer an alternative fabrication strategy. According to this methodology, silicon-based polymers, such as silicones, are converted into ceramic materials through pyrolysis (thus motivating the term 'preceramic polymers'). When combined with suitable oxide fillers, these systems can yield amorphous-crystalline composites similar to conventional glass-ceramics, without the need for a melt-derived glass precursor. The high reactivity of silica generated during the decomposition of the silicone enables in-situ crystallization, often at lower temperatures and through a single thermal treatment step [13,14].

An additional advantage of silicone-based systems is their compatibility with additive manufacturing techniques [15,16]. In particular, digital light processing (DLP), a vat photopolymerization method, allows for the shaping of complex architectures using photosensitive resins [17–19]. Printable formulations can be obtained just by physically mixing a silicone polymer with an acrylate-based resin [20]. Sodium nitrate, introduced via emulsification [20], improves dispersion stability and homogeneity, while strontium carbonate may serve as a stimulus (by supplying SrO) for specific crystalline phases [14]. When pyrolyzed under nitrogen, these formulations generate a multiphase ceramic material comprising silicate crystals within a glassy matrix [21], along with turbostratic carbon from the organic backbone [22]. This carbon phase may contribute to the electronic conductivity of the final component [23,24].

In this study, we propose a simplified processing route to obtain electrically conductive, silicate-based glass-ceramic analogues using silicone-derived preceramic formulations. The aim is to demonstrate that a single-step thermal treatment, combined with 3D printing via DLP, can yield monolithic components with structural and functional characteristics comparable to those of conventional glass-ceramics, without requiring melt-quenching or multi-stage devitrification [19,25].

2. Materials and Methods

2.1. Preparation and 3D Printing of Silicone-Based Emulsions

A key novelty of the current approach is the application of a silicone-based 'suspension-emulsion'. In fact, sodium and strontium oxide precursors could be mixed with a silicone resin (Silres® H44, Wacker Chemie AG, Munich, Germany) in two distinct stages.

An 'oily' phase was prepared by mixing 5 g of H44 with 5 g of a commercial acrylate-based photocurable resin (Industrial Blend Transparent, FunToDo, Alkmaar, The Netherlands). The two components were homogenized using a planetary mixer (Thinky ARE-250, Intertronics, Kidlington, UK) operated at 2000 rpm for 10 min.

In parallel, an 'aqueous' phase was produced by emulsifying 10 g of the same photocurable resin with 1 g of Span 80 (sorbitan mono-oleate, TCI, Tokyo, Japan) and 2.6 g of sodium nitrate ($NaNO_3$, Sigma-Aldrich, St. Louis, MO, USA). The mixture was sonicated using an ultrasonic tip device (Bandelin Sonopuls HD 2070, Berlin, Germany) for 60 min under continuous magnetic stirring. Subsequently, the emulsion was further homogenized using a high-speed planetary mixer (SmartDac 250.4 VAC-PLR, Hauschild SpeedMixer,

Hamm, Germany) with a programmed sequence of 2 min at 200 rpm, 2 min at 2200 rpm, and 4 min at 2400 rpm. After this step, 3.3 g of strontium carbonate ($SrCO_3$, Sigma-Aldrich, ≥98%) powders were suspended into the emulsion through additional sonication for 10 min to ensure uniform distribution of the ceramic filler.

The oily and aqueous phases were then combined and homogenized using the same Thinky planetary mixer for 5 min, resulting in a stable and printable ceramic precursor formulation.

Disk-shaped substrates, 30 mm in diameter and 0.7 mm in thickness, were fabricated using a masked vat-photopolymerization 3D printer (Prusa SL1S, Prusa Research, Prague, Czech Republic), operating at a wavelength of 405 nm. The printing process was conducted with a layer thickness of 50 µm and an exposure time of 5 s per layer. The platform was gradually lifted from the resin bath, forming the 3D geometry layer by layer.

After printing, the green parts were removed from the build platform and cleaned by immersion in isopropyl alcohol (IPA) for 10 s to remove residual unpolymerized resin. The samples were then post-cured under UV light (Prusa CW1, Prusa Research) at 405 nm for 10 min per side to complete polymerization.

Ceramization was achieved through a two-step heat treatment in a flowing nitrogen atmosphere. The temperature was initially raised at 0.5 °C/min up to 500 °C, with a dwell time of 2 h to induce polymer-to-ceramic conversion. This was followed by a second ramp of 1 °C/min up to 1050 °C, with an additional 2 h dwell at the maximum temperature to promote crystallization and densification of the ceramic matrix [2]. A detailed overview of the full fabrication process, including emulsion preparation, 3D printing, and thermal treatment, is provided in Appendix A.

2.2. Characterization of Printed Components and Final Substrates

The morphological features of the printed components, both before and after thermal treatment, were evaluated using optical stereomicroscopy (AxioCam microscopy camera, Carl Zeiss™, Oberkochen, Germany) to assess the overall surface quality and the structural homogeneity of internal geometries.

Detailed microstructural observations of heat-treated samples were conducted using environmental scanning electron microscopy (ESEM, FEI Quanta 200, Eindhoven, The Netherlands), equipped with an energy-dispersive X-ray spectroscopy (EDS) detector, in order to investigate phase distribution and elemental composition at the microscale.

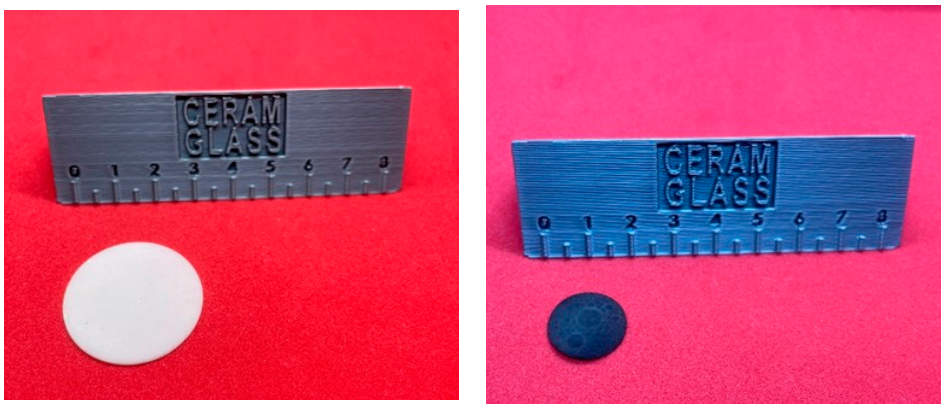
Phase identification of powdered samples, collected before and after pyrolysis, was conducted by X-ray diffraction (XRD) using a Bruker AXS D8 Advance diffractometer (Karlsruhe, Germany). Data were collected in the 2θ range of 10–60°, with a step size of 0.05° and a counting time of 1 s per step, using Cu Kα radiation and a Ni filter. Phase analysis and peak identification were performed using the Match! software package (Version 1.11h, Crystal Impact GbR, Bonn, Germany).

To verify the conduction of electricity, a digital multimeter was utilized to measure the resistance of the material.

3. Results and Discussion

3.1. Morphological Evolution Before and After Thermal Treatment

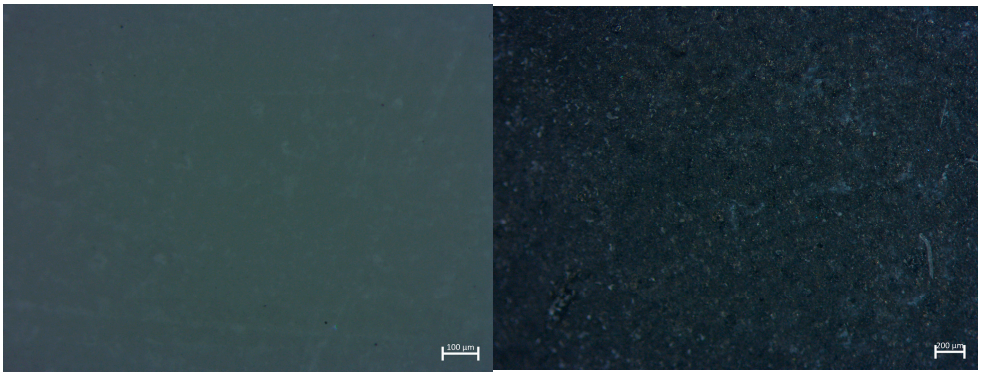
The green parts produced using DLP printing had smooth, defect-free surfaces and good dimensional accuracy (Figure 1a), which confirms that the silicone-acrylate formulation with oxide precursors has adequate photoreactivity and dispersion stability. No significant filler sedimentation or phase separation occurred prior to heat treatment.



(**a**) (**b**)

Figure 1. (**a**) Green 3D-printed sample before pyrolysis; (**b**) Same sample after heat treatment at 1050 °C in N_2, showing black coloration and shrinkage.

Following pyrolysis at temperatures up to 1050 °C in an inert atmosphere, the parts shrank substantially and changed colour to opaque black (Figure 1b). This was attributed to the ceramization of the silicone matrix and the formation of a pyrolytic carbon phase. Macrostructural heterogeneity was observed on the surface as a consequence gas-induced bubbles clearly visible under optical stereomicroscopy (Figure 2).



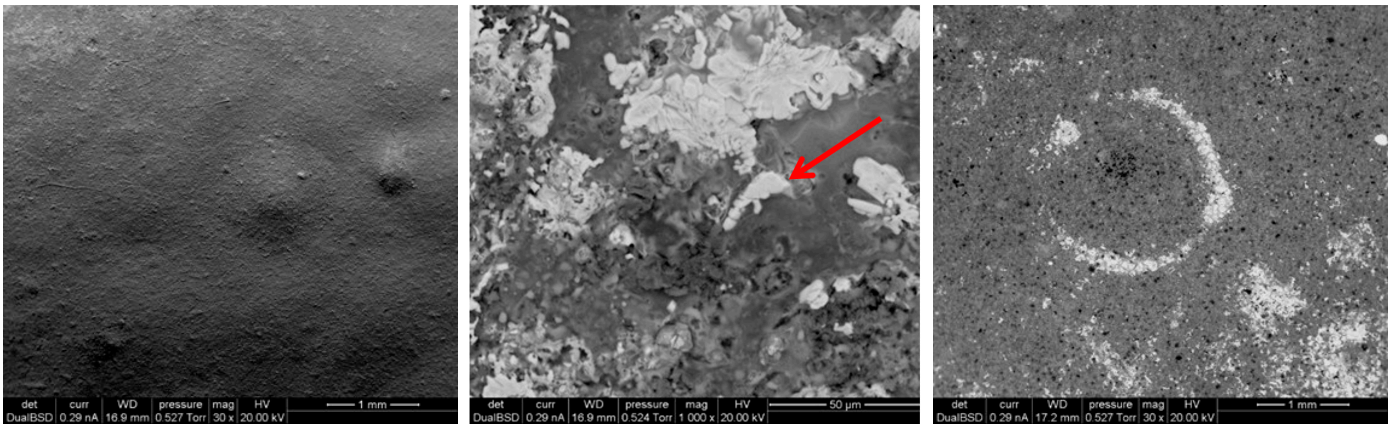
(**a**) (**b**)

Figure 2. Optical stereomicroscope images: (**a**) Surface of green part with uniform texture; (**b**) Fired part showing bubbles due to internal gas pressure during pyrolysis.

These bubbles are likely the result of internal gas pressure build-up during the decomposition of $NaNO_3$ and $SrCO_3$, coupled with limited gas diffusion through the already polymerised outer shell. This phenomenon is common in polymer-derived ceramic systems, particularly in geometries with limited wall thickness and restricted gas escape pathways [22].

Interestingly, elemental mapping by EDX revealed that strontium tends to concentrate within or around these bubbles, suggesting a degree of phase separation or differential diffusion during ceramic transformation. One hypothesis is that Sr-containing species (e.g., SrO or Sr^{2+} complexes) migrate towards low-density or low-viscosity regions during the initial stages of pyrolysis, possibly facilitated by localised gas flow or melt-phase redistribution prior to crystallisation.

Such preferential accumulation could influence local crystallisation behaviour, explaining the presence of Sr-rich crystallites at bubble perimeters as observed under SEM and EDX (Figures 3b and 4).



(**a**) (**b**) (**c**)

Figure 3. SEM micrographs at increasing magnifications showing: (**a**) Surface morphology of glass-ceramic composite; (**b**) Elongated $SrSiO_3$ crystallites (the arrow indicates an elongated $SrSiO_3$ crystallite); (**c**) Detail of intergranular bubble and strontium-rich zones.

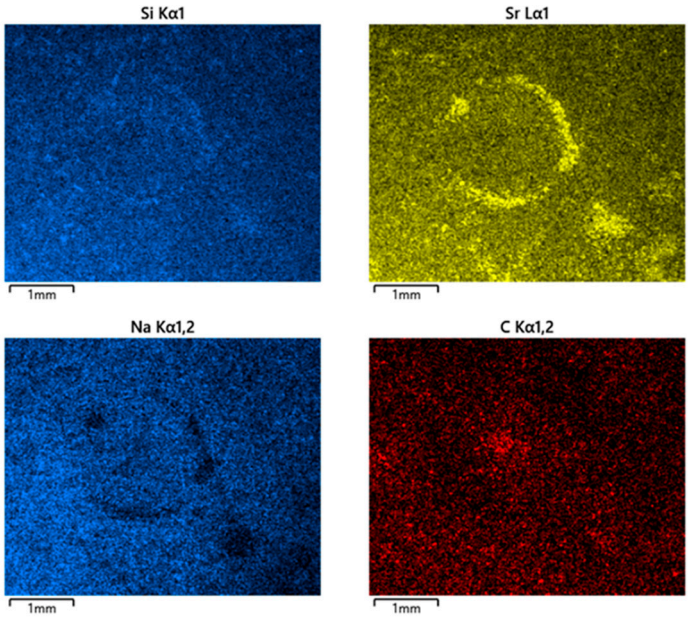


Figure 4. EDX map focuses on a bubble zone. Si (light blue), Sr (yellow), Na (blue), and C (red). Brighter areas indicate higher concentrations of the respective elements.

3.2. Microstructure and Elemental Distribution (SEM-EDX)

SEM analysis (Figure 3) revealed a heterogeneous microstructure composed of dense ceramic regions. At higher magnifications, elongated and plate-like crystalline grains could be distinguished embedded in a darker matrix, which is presumably amorphous.

EDX mapping confirmed a relatively uniform distribution of silicon, oxygen and carbon throughout the matrix. As Figure 4 shows, the EDX map highlights strontium accumulation along the bubble boundaries, indicating preferential segregation of strontium in these areas. This supports the observation of strontium-rich crystallites near pore boundaries. Localised strontium enrichment in pore-rich regions (Figure 5 and Table 1). Although this indicates that the distribution of strontium is not homogeneous at the microscopic level, the composition of the matrix remains relatively uniform. This heterogeneity is likely related to the foaming phenomena that occur during pyrolysis and must therefore be considered an intrinsic feature of the current processing route. The turbostratic carbon

phase is attributed to the decomposition of the organic resin in nitrogen, and it provides potential pathways for electronic conductivity.

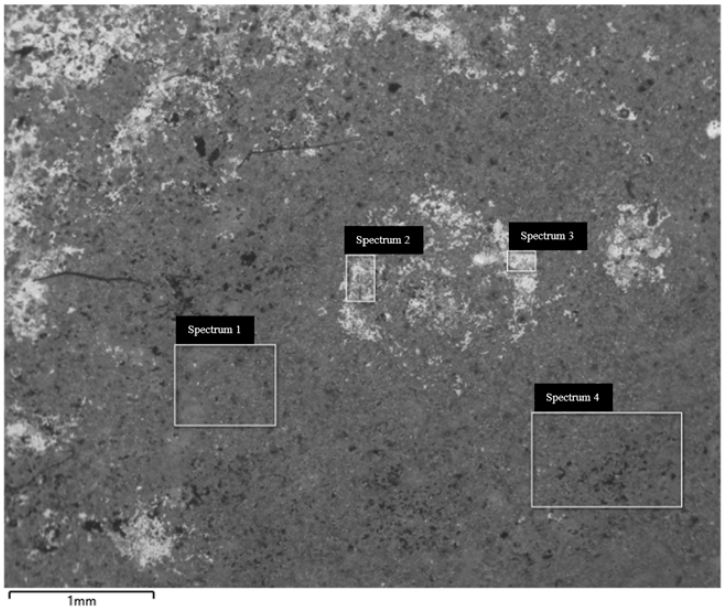


Figure 5. EDX spectrum analysis of different zones of the surface.

Table 1. EDX spectrum analysis of different zones of the surface.

	% wt.			
Element	**Spectrum 1**	**Spectrum 2**	**Spectrum 3**	**Spectrum 4**
C	23.2	21.4	19.2	24.6
Sr	8.1	19.1	26	7.5
Na	11.7	8.8	6.3	12.6
Si	13.6	11.6	11.7	12
O	42.7	38.6	36.9	42.8

The absence of residual sodium peaks in the EDX data and the lack of clear Na-containing crystalline phases suggests that either $NaNO_3$ volatilised during pyrolysis or that amorphous sodium silicate domains formed below XRD detectability. NMR or XPS studies would be required to further clarify the sodium speciation, but they are beyond the scope of the present paper.

3.3. Phase Evolution by X-Ray Diffraction

The XRD pattern of the heat-treated samples (Figure 6) confirmed that the dominant crystalline phase was $SrSiO_3$. All the major peaks matched those of the orthorhombic polymorph of strontium metasilicate, which is consistent with the literature. The broad hump between 20° and 35° 2θ indicates an amorphous silicate background.

Notably, no peaks corresponding to sodium-containing phases were detected. Furthermore, no reflections associated with residual $SrCO_3$ or $NaNO_3$ could be observed, confirming that the samples underwent complete reaction and conversion during thermal treatment, in line with the fact that $SrCO_3$ decomposes above 875 °C and $NaNO_3$ decomposes above 450 °C.

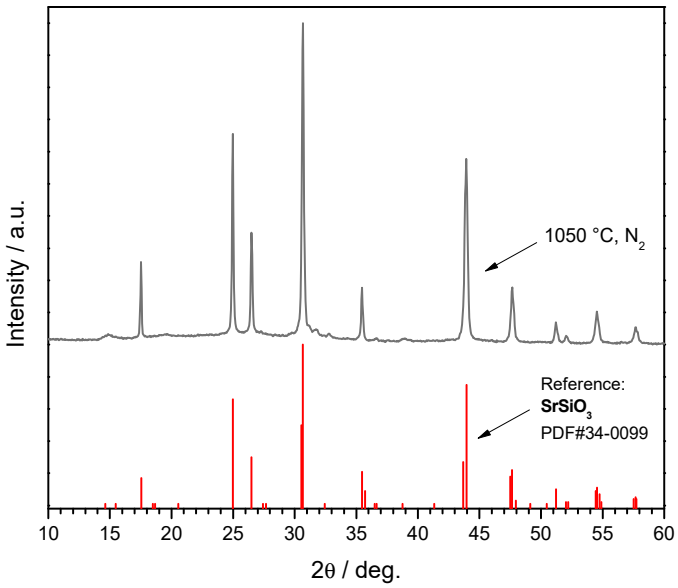


Figure 6. XRD pattern of the final ceramic showing dominant $SrSiO_3$ peaks and an amorphous background.

3.4. Electrical Behaviour

Contact probe measurements using a digital multimeter verified that the pyrolyzed samples were electrically conductive. This confirms the development of a conductive network within the ceramic body.

The observed conductivity is attributed to a dual mechanism involving the pyrolytic carbon phase formed from the decomposition of the silicone backbone in an inert atmosphere and the crystalline $SrSiO_3$ phase which is known in the literature to exhibit semiconducting behaviour, particularly when formed in non-stoichiometric or defect-rich environments.

The presence of $SrSiO_3$, as confirmed by XRD, may enhance electrical conduction via hopping or small-polaron mechanisms [26], particularly if point defects (e.g., Sr or oxygen vacancies) are introduced during processing. Such defects are commonly generated in polymer-derived ceramic systems due to the non-equilibrium nature of the ceramization route and rapid gas release.

Furthermore, the partial connectivity of the pyrolytic carbon phase can improve electron transport across grain boundaries or through residual glassy regions. The carbon is likely to exist in a turbostratic or amorphous form [27]. While this is less conductive than graphitic carbon, it can still support percolation paths when sufficiently interconnected.

This glass-ceramic composites microstructure, comprising conductive ceramic crystals and a dispersed carbon network, suggests that the resulting material behaves as a mixed electronic conductor. These characteristics could be exploited in applications requiring electronic transport at moderate temperatures, such as in electrodes, gas sensors or interconnect materials in solid-state devices.

4. Conclusions

A simplified processing route has been developed for fabricating electrically conductive silicate-based glass-ceramic composites starting from printable, silicone-derived emulsions. A mixture of silicone resin, acrylate-based photocurable resin, sodium nitrate and strontium carbonate was found to enable the formation of stable, photoreactive formulations that were suitable for shaping via digital light processing (DLP).

Following a single-step thermal treatment in nitrogen, the green bodies were converted into glass-ceramic composites structures consisting of $SrSiO_3$ crystals embedded in an amorphous matrix containing dispersed turbostratic carbon. This microstructure was confirmed by SEM, EDX and XRD analyses and resulted in electrically conductive materials. This conductive behaviour is attributed to the presence of the semiconducting material $SrSiO_3$ and to the formation of an interconnected carbon phase originating from the silicone matrix.

Despite heterogeneity on the surface developing due to gas evolution during nitrate decomposition, the fired substrates maintained sufficient mechanical integrity. These characteristics suggest potential applications in functional ceramics requiring moderate electronic conductivity.

This study demonstrates the feasibility of producing conductive glass-ceramic analogues without the need for traditional glass melting or multi-step crystallisation. In line with previous studies on polymer-derived ceramics, which recognised the potential of crystallisation within an amorphous precursor matrix to tailor microstructures, this work demonstrates the direct application of this approach in silicate-based systems. The incorporation of crystalline $SrSiO_3$ domains within an amorphous Si–O–C matrix via a simplified, one-step process demonstrates the potential of polymer-to-ceramic strategies in producing functional glass-ceramic composites without the need for conventional melting. This advancement extends the concept of crystalline-phase-containing PDCs to electrically conductive, additively manufactured systems, revealing new possibilities for functional ceramic technologies. Future investigations will include quantitative electrical characterisation, surface heterogeneity reduction and stability assessment under operational conditions.

Author Contributions: Conceptualization, A.Z. and E.B.; methodology, E.B.; software, E.B.; validation, A.Z. and E.B.; formal analysis, A.Z.; investigation, A.Z.; resources, E.B.; data curation, A.Z.; writing—original draft preparation, A.Z.; writing—review and editing, E.B.; visualization, E.B.; supervision, E.B.; project administration, E.B.; funding acquisition, E.B. All authors have read and agreed to the published version of the manuscript.

Funding: This research was funded by Italian Ministry of University and Research (MUR) by means of National Recovery Funds (PNRR), through DM117/2023 PhD Scholarship Program. The authors acknowledge the co-funding from DeAngeli Prodotti S.r.l. (Bagnoli di Sopra, Italy).

Data Availability Statement: The original contributions presented in this study are included in the article material. Further inquiries can be directed to the corresponding author.

Acknowledgments: A.Z. and E.B. ackwnoledge Nicola Bianchi and Renato Gobbo (Department of Industrial Engineering) for experimental assistance.

Conflicts of Interest: The authors declare no conflicts of interest.

Appendix A

The Figure A1 provides a visual summary of the fabrication process used to produce conductive glass-ceramic components from a silicone-based printable formulation. The process begins with the preparation of a multifunctional mixture comprising a silicone resin, a photocurable acrylate resin, sodium nitrate ($NaNO_3$) and strontium carbonate ($SrCO_3$). Adding a surfactant ensures the system is properly dispersed and stabilized, enabling the formation of a homogeneous emulsion.

In this formulation, sodium nitrate is present in liquid form while strontium carbonate is present as solid particles. The silicone and photocurable resin create an organic matrix that can be structured via photopolymerization. Once mixed, the emulsion exhibits sufficient rheological and optical properties to be processed using digital light processing

(DLP), a 3D printing technique that enables the composite to be shaped layer by layer into complex geometries.

After printing, the 'green' components, which are still polymeric, undergo UV post-curing to complete the polymer cross-linking and ensure structural stability prior to firing. Subsequent heat treatment under nitrogen initiates a twofold transformation. First, the silicone undergoes ceramization to form a partially amorphous silicate matrix. Secondly, the added inorganic components participate in solid-state reactions. $SrCO_3$ reacts with silica to form crystalline strontium silicate ($SrSiO_3$), while $NaNO_3$ either volatilizes or contributes to the formation of sodium-containing amorphous domains.

At the same time, the organic components of the matrix decompose, resulting in the formation of a turbostratic carbon phase. This phase remains embedded within the ceramic and contributes to the final material's overall electronic conductivity.

The result is a glass-ceramic microstructure comprising $SrSiO_3$ crystals dispersed in a silica-based matrix and a percolative network of conductive carbon residues. Interactions between sodium, strontium and silicon oxides during thermal processing are crucial for defining the final phase composition and electrical properties of the material.

This processing route offers a more efficient alternative to conventional glass-ceramic fabrication by eliminating the need for prior glass melting and enabling direct shaping via additive manufacturing techniques. This opens up new possibilities for designing conductive ceramic components with complex geometries and functional performance tailored to electronic or electrochemical applications.

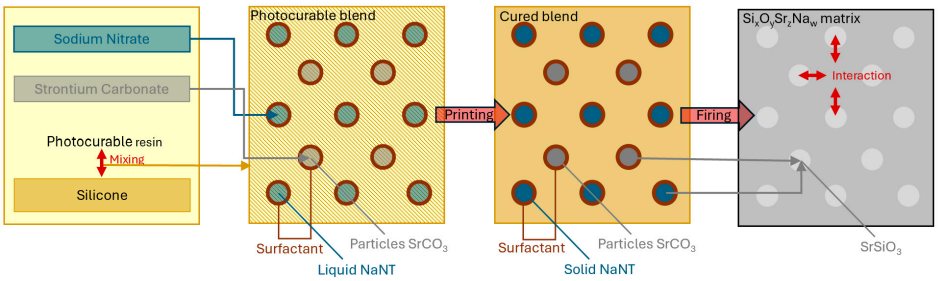


Figure A1. The fabrication process involves silicone-based precursor formulation, 3D printing, UV curing and high-temperature treatment. This results in a conductive glass-ceramic material containing $SrSiO_3$ crystals and turbostratic carbon.

References

1. Pietrzak, T.K.; Wasiucionek, M.; Garbarczyk, J.E. Towards higher electric conductivity and wider phase stability range via nanostructured glass-ceramics processing. *Nanomaterials* **2021**, *11*, 1321. [CrossRef]
2. Smeacetto, F.; Saffirio, S.; Salvo, M.; Palliotto, A.; Zhang, J.; De Angelis, S.; Tinti, V.B.; Esposito, V. Fast-quenched $Na_2Si_2O_5$ stability and properties in crystalline composite. *Materialia* **2023**, *33*, 101968. [CrossRef]
3. Singh, P.; Goodenough, J.B. $Sr_{1-x}K_xSi_{1-y}Ge_yO_{3-0.5x}$: A new family of superior oxide-ion conductors. *Energy Environ. Sci.* **2013**, *6*, 176–180. [CrossRef]
4. Singh, P.; Goodenough, J.B. Monoclinic $Sr_{1-x}Na_xSiO_{3-0.5x}$: New superior oxide ion conductors. *J. Am. Chem. Soc.* **2013**, *135*, 4258–4263. [CrossRef]
5. Evans, J.S.O. Polanyi-like formulations for rapidly predicting key thermodynamic and kinetic parameters. *Chem. Mater.* **2015**, *27*, 8485–8491. [CrossRef]
6. González Puente, P.M.; Song, S.; Cao, S.; Rannalter, L.Z.; Pan, Z.; Xiang, X.; Shen, Q.; Chen, F. Garnet-type solid electrolyte: Advances of ionic transport performance and its application in all-solid-state batteries. *J. Adv. Ceram.* **2021**, *10*, 933–972. [CrossRef]
7. Wu, H.; Zhuo, D.; Kong, D.; Cui, Y. Improving battery safety by early detection of internal shorting with a bifunctional separator. *Nat. Commun.* **2014**, *5*, 5193. [CrossRef]
8. Gao, L.; Li, Q.; Sun, L.; Zhang, X.; Huo, L.; Zhao, H.; Grenier, J.-C. A novel family of Nb-doped $Bi_{0.5}Sr_{0.5}FeO_3-\delta$ perovskite as cathode material for intermediate-temperature solid oxide fuel cells. *J. Power Sources* **2017**, *371*, 86–95. [CrossRef]
9. Ti Jee, Y.; Zhao, X.; Huang, K. On the cause of conductivity degradation in sodium strontium silicate ionic conductor. *Chem. Commun.* **2015**, *51*, 9640–9642. [CrossRef] [PubMed]

10. Zanotto, E.D. A bright future for glass-ceramics. *Am. Ceram. Soc. Bull.* **2010**, *89*, 19–27.
11. Jee, Y.; Zhao, X.; Lei, X.; Huang, K. Phase relationship and ionic conductivity in Na–$SrSiO_3$ ionic conductor. *J. Am. Ceram. Soc.* **2016**, *99*, 324–330. [CrossRef]
12. Riedel, R.; Mera, G.; Hauser, R.; Klonczynski, A. Silicon-based polymer-derived ceramics: Synthesis, properties and applications—A review. *J. Ceram. Soc. Jpn.* **2006**, *114*, 425–444. [CrossRef]
13. Colombo, P.; Mera, G.; Riedel, R.; Sorarù, G.D. Polymer-derived ceramics: 40 years of research and innovation in advanced ceramics. *J. Am. Ceram. Soc.* **2010**, *93*, 1805–1837. [CrossRef]
14. Bernardo, E.; Fiocco, L.; Parcianello, G.; Storti, E.; Colombo, P. Advanced Ceramics from Preceramic Polymers Modified at the Nano-Scale: A Review. *Materials* **2014**, *7*, 1927–1956. [CrossRef]
15. Travitzky, N.; Bonet, A.; Dermeik, B.; Fey, T.; Filbert-Demut, I.; Schlier, L.; Schlordt, T.; Greil, P. Additive manufacturing of ceramic-based materials. *Adv. Eng. Mater.* **2014**, *16*, 729–754. [CrossRef]
16. Zocca, A.; Colombo, P.; Gomes, C.M.; Günster, J. Additive manufacturing of ceramics: Issues, potentialities, and opportunities. *J. Am. Ceram. Soc.* **2015**, *98*, 1983–2001. [CrossRef]
17. Schmidt, J.; Colombo, P. Digital light processing of ceramic components from polysiloxanes. *J. Eur. Ceram. Soc.* **2018**, *38*, 57–66. [CrossRef]
18. Chaudhary, R.P.; Parameswaran, C.; Idrees, M.; Rasaki, A.S.; Liu, C.; Chen, Z.; Colombo, P. Advanced ceramics from polymer-derived ceramics: Synthesis, properties, and applications. *Prog. Mater. Sci.* **2022**, *128*, 100969. [CrossRef]
19. Eckel, Z.C.; Zhou, C.; Martin, J.H.; Jacobsen, A.J.; Carter, W.B.; Schaedler, T.A. Additive manufacturing of polymer-derived ceramics. *Science* **2016**, *351*, 58–62. [CrossRef]
20. Elsayed, H.; Stabile, F.M.; Savio, G.; Bernardo, E. Masked stereolithography of wollastonite-diopside glass-ceramics from novel silicone-based liquid feedstock. *Open Ceram.* **2023**, *16*, 100474. [CrossRef]
21. Höland, W.; Beall, G.H. *Glass-Ceramic Technology*, 3rd ed.; Wiley: Hoboken, NJ, USA, 2019. [CrossRef]
22. Colombo, P. Engineering porosity in polymer-derived ceramics. *J. Eur. Ceram. Soc.* **2008**, *28*, 1389–1395. [CrossRef]
23. Walters, C.C.; Kliewer, C.E.; Awwiller, D.N.; Rudnicki, M.D.; Passey, Q.R.; Lin, M.W. Influence of turbostratic carbon nanostructures on electrical conductivity in shales. *Int. J. Coal Geol.* **2014**, *122*, 105–109. [CrossRef]
24. Monthioux, M. Describing carbons. *Carbon Trends* **2024**, *14*, 100325. [CrossRef]
25. Lacelle, T.; Sampson, K.L.; Yazdani Sarvestani, H.; Rahimizadeh, A.; Barroeta Robles, J.; Mirkhalaf, M.; Rafiee, M.; Jakubinek, M.B.; Paquet, C.; Ashrafi, B. Additive manufacturing of polymer-derived ceramics: Materials, methods, and applications. *APL Mater.* **2023**, *11*, 070602. [CrossRef]
26. Kreuer, K.D. Proton-conducting oxides. *Annu. Rev. Mater. Sci.* **2003**, *33*, 333–359. [CrossRef]
27. Bo, X.; Li, M.; Han, C.; Zhang, Y.; Nsabimana, A.; Guo, L. Noble metal-free electrocatalysts for the oxygen reduction reaction based on iron and nitrogen-doped porous graphene. *J. Mater. Chem. A* **2015**, *3*, 1058–1067. [CrossRef]

Disclaimer/Publisher's Note: The statements, opinions and data contained in all publications are solely those of the individual author(s) and contributor(s) and not of MDPI and/or the editor(s). MDPI and/or the editor(s) disclaim responsibility for any injury to people or property resulting from any ideas, methods, instructions or products referred to in the content.